GPS Solutions (2025) 29:111
https://doi.org/10.1007/s10291-025-01861-5

RESEARCH

Deep learning approach for combining global ionospheric maps for GNSS positioning

Mateusz Poniatowski[1,3] · **Grzegorz Nykiel**[2,3,4] · **Mohammed Mainul Hoque**[4] · **Jędrzej Szmytkowski**[1]

Received: 9 September 2024 / Accepted: 8 April 2025

Abstract

One of the most widely used sources for information regarding the state of the ionosphere is the global ionospheric maps provided by the IGS service. These maps are created through a weighted average of solutions from various centers, including CODE, ESA, JPL and UPC. As technology has advanced, the application of artificial intelligence in ionospheric research has become more prevalent, motivating us to apply this approach to improve the process of combining ionospheric maps. The objective of our research is to use deep learning in the form of recurrent neural networks to generate global ionospheric maps. The model is complemented by the inclusion of positional and temporal parameters as well as solar and geomagnetic activity indices. In the study, the total electron content (TEC) was extracted from Jason altimetry measurements that served as the reference data for the model. The Jason TECs contain electron content up to an orbit height of approximately 1336 km. Therefore the missing data above the Jason orbit was modelled using several ionospheric/plasmaspheric models. One of the key objective of this study was to identify the optimal fitting model for mapping electron content above the Jason orbit. The solution that demonstrate the most significant impact on the learning process and providing the best results was the Neustrelitz Electron Density Model (NEDM). To validate the Gdańsk University of Technology model (GUT), we conducted a comparative analysis of single-frequency positioning using maps from GUT and IGS. Our solution demostrated an improvement in positioning for over 70% out the 300+ stations studied on average for each studied day during calm or disturbed ionospheric conditions. For three-dimensional positioning errors, we obtained improvements ranging from 5 to 15% relative to IGS results.

Keywords GNSS · IGS · Ionospheric maps · Deep learning · TEC · Positioning

Introduction

The ionosphere is a key layer of the atmosphere that directly affects our daily lives. High frequency signals are reflected back at the bottom ionosphere what is the core element to long-distance radio communication. Ionosphere also affects information transmission between ground receivers and satellites. The distance traveled by a radio wave on the satellite-receiver path is extended/shortened by ionospheric propagation effects when passing through media with different electron densities. Ionosphere is a very dynamic medium controlled by the space weather. It is necessary to constantly monitor it to reduce its influence on signal propagation, which is particularly important in a satellite communications. The distance traveled by a radio wave on the satellite-receiver path is extended by multiple refraction of the signal that is passing through media with different electron densities. This also contributes to sudden changes in signal strength which might result in signal fading. There-

✉ Mateusz Poniatowski
mateusz.poniatowski@pg.edu.pl

Grzegorz Nykiel
grzegorz.nykiel@dlr.de

Mohammed Mainul Hoque
mainul.hoque@dlr.de

Jędrzej Szmytkowski
jedrzej.szmytkowski@pg.edu.pl

[1] Faculty of Applied Physics and Mathematics, Gdańsk University of Technology, Narutowicza 11/12, 80-233 Gdańsk, Poland

[2] Faculty of Civil and Environmental Engineering, Gdańsk University of Technology, Narutowicza 11/12, 80-233 Gdańsk, Poland

[3] Digital Technologies Center, Gdańsk University of Technology, Narutowicza 11/12, 80-233 Gdańsk, Poland

[4] Institute for Solar-Terrestrial Physics, German Aerospace Center (DLR), Neustrelitz, Germany

fore, it is important to know the state of the ionosphere. Over the years, a number of models have been developed to conduct research on this layer of the atmosphere. Such models are, for example, the Field Line Interhemispheric Plasma (FLIP) (Richards 35), The Global Assimilation of Ionospheric Measurements-Gauss Markov (GAIM-GM) (Gardner et al. 12), the Thermosphere Ionosphere Electrodynamic General Circulation Model (TIEGCM) (Qian et al. 33). In addition to models focusing on study of the physical aspects of the ionosphere, others have also been developed to describe the state of electron density. These models have been primarily developed to eliminate the first-order ionospheric delay on single-frequency measurements, which, unlike dual-frequency measurements, lack the ability to compensate for it by using a linear combination of ionosphere-free data at L1 and L2 frequencies (Liu et al. 22). Additionally, these models serve as an excellent source of data to further study the state and variability of the ionosphere.

The models that are commonly used to reduce the impact of the ionosphere on single-frequency satellite signals are shown in Table 1. The Klobuchar model is still used to provide an ionospheric correction for GPS measurements. A similar application is found in the NeQuick2 model, with one version (NeQuick G) employed by ESA for Galileo satellites. NeQuick 2 has also been implemented as a proposed ionosphere model in recommendation ITU-R P.531. The International Reference Ionosphere (IRI) is a model that finds global application in climatology and in prediction of the state of the ionosphere (Bilitza et al. 2). An extension of this model is the IRI Real-Time Assimilative Mapping (IRTAM), which employs a network of ionosondes to obtain additional data regarding the vertical profiles (Galkin et al. 11). Models from CODE, ESA, JPL and UPC centers provide information on the global state of the ionosphere. Data for these maps are collected via a network of ground stations conducting continuous GNSS measurements, enabling the determination of slant total electron content (STEC) along signal paths. These STEC values are then converted to vertical TEC and employed to produce final maps by the IGS, utilizing a straightforward method involving weighted averages of the input maps. These weights are derived by the evaluation center (UPC), computed from the inverse root mean square error of STEC reproduction. For validation, the IGS uses TEC information extracted from altimetry missions data, in past from Topex/Poseidon, nowadays from Jason (Hernández-Pajares et al. 17). The resulting combined products are the final maps, typically available approximately two weeks after measurement collection, generated as a two-hour interval map in IONosphere Map EXchange format version (IONEX) format (Schaer et al. 37) Due to its high quality, the IGS solution is widely utilized for reducing ionospheric delays impact on GNSS measurements in postprocessing.

The development of machine learning and its ability to uncover hidden connections between parameters have been utilized for many years to study the state of the ionosphere and predict its behavior. In the literature, numerous studies can be found that focus on predicting TEC using deep learning algorithms (Huang and Yuan 19; Razin et al. 34; Wen et al. 41). The development of fundamental machine learning algorithms for TEC prediction and modeling has also gained popularity (Zhukov et al. 47; Razin et al. 34). However, there are only a few works dedicated to creating algorithms that fuse ionospheric maps using methods other than the weighted average approach employed by the IGS. One approach to combining products that describe the state of the ionosphere into a single final product involves the use of hybrid deep learning to integrate maps extracted from the Massachusetts Institute of Technology (MIT), the IGS, and TEC derived from altimetry measurements (Chen et al. 3). By combining products with different coverage areas (IGS - global; MIT - continents and coastal regions; altimetry - ocean measurements), satisfactory results were achieved, yielding a highly accurate solution.

Artificial intelligence algorithms serve as valuable tools in modeling the state of the ionosphere. Consequently, we decided to explore their utility in the process of merging the products included in the IGS solution. The challenge associated with fusing global ionospheric maps from CODE, ESA, JPL and UPC centers lies in their multidimensional character. We encounter variations in space (geographic longitude, latitude and solar zenith angle) and in time (diurnal, seasonal, and solar cycle-related). In addition, modeling of the agitated state of the ionosphere, especially during extreme geomagnetic disturbances, is a problem. The main factor inducing disturbances in the atmospheric layer in question is coronal mass ejections from the Sun (Peng et al. 30), which result in shocks to the Earth's magnetic field, leading to geomagnetic storms (Wu et al. 42; Gonzalez et al. 15). The stronger the phenomenon, the more severe its effects on the positioning process (Poniatowski and Nykiel 31; Luo et al. 23). Correctly combining maps for days on which geomagnetic storms occurred is crucial and also problematic due to the small amount of available data describing the agitated state of the ionosphere in the learning set. The objective of our research was to determine whether deep learning techniques could address the aforementioned challenges and assess the quality of our solution in comparison to the IGS product. Accordingly, we decided to integrate of maps from IAAC centers with local information (time, position, TEC value) and global information (solar and geomagnetic activity indices). In our work, we propose a deep learning-based approach to ionospheric modeling that aims to improve GNSS positioning accuracy by capturing complex, non-linear spatio-temporal patterns between input GIMs. While our method differs in input, structure, and technique from the final IGS product,

Table 1 Common models representing state of the ionosphere utilized in elimination of first-order ionospheric delay for single-frequency receivers

Product	Reference	Main modeling technique
Klobuchar	[20]	Empirical approach with thin-single-layer of the ionosphere
Center for Orbit Determination in Europe (CODE)	[36]	Single-layer approach using spherical harmonics of degree 15
Jet Propulsion Laboratory (JPL)	[24]	3D-Triangulation based on tessellation of a sphere
Polytechnic University of Catalonia (UPC)	[16]	Tomographic method
European Space Agency (ESA)	[10]	Single-layer approach using spherical harmonics of degree 15
NeQuick2	[27]	5 semi-Epstein layers with thickness modeling
International GNSS Service (IGS)	[17]	Weighted average
Natural Resources Canada (NRCan)	[14]	Spherical harmonics
Wuhan University (WHU)	[46]	Spherical harmonics of degree 15 with inequality-constrained least squares
Chinese Academy of Science (CAS)	[21]	Spherical harmonics with generalized trigonometric series
NeQuick G	[7]	The bottom layer of the model is composed of three Epstein layers, while the topside consists of a semi-Epstein layer with a correction for an exosphere electron density
International Reference Ionosphere (IRI)	[2]	Six sub-regions; for each of them different model is applied
NTCM G	[8]	Empirical approach focusing on five major components: local time and seasonal dependency, geomagnetic field and solar activity dependency, equatorial anomaly dependency

the comparison between them will provide a useful insight into the strengths of a data-driven approach.

Data

Global ionospheric maps

In our work, we focused on combining available ionospheric maps from IAAC centers that contribute to the IGS solution, namely products from CODE, ESA, JPL and UPC centers. The CODE solution is based on the use of a single layer model of the ionosphere of infinitesimal thickness using spherical harmonics of degree 15 (Schaer et al. 36). A similar method is used by the ESA center (Feltens 9, 10). The JPL center, on the other hand, uses a three-dimensional triangulation approach by tessellating the sphere at a certain height. The model also uses bilinear splines to represent the TEC distribution (Mannucci et al. 24). The UPC model, on the other hand, uses a tomographic method based on phase measurements. It is a two-layer solution (layer one: 60–740 km; layer two: 740–1420 km). In this solution the surface of the ionosphere is divided into cells with size of $5^\circ \times 2.5^\circ$ or $10^\circ \times 5^\circ$, in which the electron density is constant (Hernández-Pajares et al. 16).

For the purpose of our study, we collected global ionospheric maps over a 16-year period (2005–2021). The dataset was prepared on the basis of a set obtained from studies on the spatio-temporal distribution of ionospheric maps and altimetry TEC (Poniatowski et al. 32). Based on these studies, we were able to identify similarities and differences between maps from IAACs and Jason-derived TEC. Results of this studies allowed us to identify Jason-TEC as high-quality source that can be used as a reference to train our model.

JASON

The basis of our learning set is the Jason-derived TEC. The main purpose of the altimetry measurements is to study the seas and oceans. However, the data from these missions is also a very good source of information on the state of the ionosphere. Based on the nature of altimetry measurements, our training set contains only data over aquatic regions. We used the data from three Jason missions: Jason-1 (2001–2013), Jason-2 (2008–2019) and Jason-3 (2016–still in use). Each of the altimeter satellites is equipped with a GPS receiver and Doppler Orbitography and Radiopositioning Integrated by Satellite system (DORIS). With the data obtained from dual-frequency (Ku-band and C-band) altimetry measurements, it is possible to determine the vertical TEC between ocean surface and Jason orbit (Yasukevich et al. 44; Scharroo and Smith 38).

$$TEC = \frac{f_{Ku}^2 f_C^2}{f_{Ku}^2 - f_C^2} \frac{R_C - R_{Ku}}{k_u} \tag{1}$$

where f_{Ku} and f_C are the frequencies at Ku-band and C-band in GHz, respectively, R_{Ku} and R_C are the distances measured in meters at Ku-band and C-band respectively, and ku is a constant of 0.403 m GHz^2 TECU^{-1}. We obtained already calculated TEC values from altimetry missions from the OpenADB service (Dettmering et al. 5) (https://openadb.dgfi.tum.de/) with a 1 s resolution. The resulting TEC is noisy and it is related to the significant difference between the two frequencies: Ku-band (waveband set to 13.575 GHz with a bandwidth of 350 MHz) and C-band (waveband of 5.3 GHz with a bandwidth of 320 MHz) (Nencioli 28). Equally important is the correction for Sea State Bias (SSB), which includes electromagnetic bias associated with wave crest reflectivity, skewness bias related to non-linear wave dynamics, and tracker bias linked to satellite tracking and instrumental errors (Badulin et al. 1). To smooth our dataset, we used a 30-s moving average with data break detection. Altimeter data are available only for seas and oceans, so encountering land creates a break in the data. Some of them span from a few to tens of degrees of latitude, resulting in a significant change in TEC. Therefore, we took this into account in the calculations. To standardize and eliminate the bias between altimetry missions, we used information from calibration periods and then aligned the data to Jason-3F mission level (Poniatowski et al. 32). Between Jason-2D and Jason-1E we obtained bias of 3.22 ± 2.84 TECU, where between Jason-3F and Jason-2D it is equal to −3.97 ± 2.23 TECU. The data was subsequently re-sampled every 5 min. We implemented this to reduce the computing power required for model learning process, while maintaining good spatial coverage. In addition, the influence of the plasmasphere above Jason's orbit also had to be taken into account. For this purpose, we used the NEDM model (Hoque et al. 18) to generate a correction above an altitude of 1336 km. The TEC correction was calculated as an integration of the profile up to 10000 km altitude with a step every 10 km. The F10.7 index was also used as an external indicator of solar activity.

Methodology

In order to create a model that allows the fusion of ionospheric maps from individual IAACs, we used a deep learning technique known as standard recurrent learning. This technique allowed us to detect connections between the temporal and spatial variability of the points on which the model was trained. To construct a suitable learning set, it was essential to understand the desired links we aimed to obtain in the model and ensure an adequate amount of data (Geron 13). The data should be carefully selected to unambiguously describe the reference value, as the selection of reference values forms the foundation of the model and greatly influences the algorithm's performance.

When addressing a spatio-temporal problem, the data considered during the learning process must appropriately represent these characteristics. The training set consists of features describing location, time, solar activity, and corresponding TEC values from individual IAACs. We used Jason-derived TEC as a reference data. Final product data from each IAACs (CODE, ESA, JPL, UPC) were linearly interpolated into altimeter satellite position and time, and incorporated as features in the deep learning model.

One of the issues encountered in creating the dataset was the date line transition. Longitudes range from −180° to 180°, where the ionospheric conditions at a given latitude can be very similar or identical at the extreme ends of the longitude range. To address this, we opted to convert longitudes to trigonometric functions of sine and cosine. A similar approach was adopted for UTC time. As for latitude, it was converted to radians. In addition, we added another positional parameter, the solar zenith angle. The parameters that had the greatest impact on the quality of the model were Kp parameter, which is a global indicator of geomagnetic activity, and the F10.7 index, which describes the level of solar radiation.

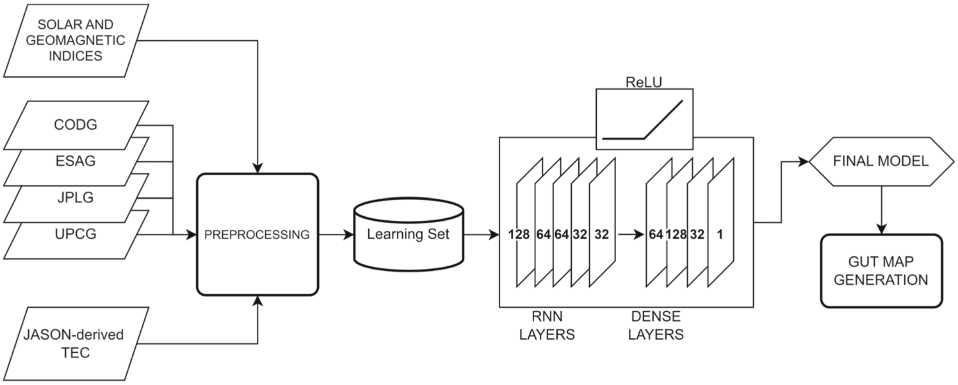

Fig. 1 Diagram showing the process of creating global ionospheric maps from the GUT model

Machine learning

Since the ionosphere is a heterogeneous layer with irregular variability, an algorithm was needed to combine multiple features and assign a single value to such a set of features. The calculations were based on tools available in the Keras and scikit-learn libraries (Pedregosa et al. 29; Chollet et al. 4). To solve this complicated problem, we decided to use deep machine learning, specifically recurrent neural networks. Many structures were tested, however, in order to minimize the chance of overfitting while maintaining very good model quality. Model was trained for 50 epochs with a batch-size of 64. The initial layers consist of a 5 recurrent layer with 128, 2 × 64, 2 × 32 neurons and rectified linear unit (ReLU) activation function. This is followed by four dense layers for regression, with 64, 128, 32 neurons and ReLU activation function, culminating in 1 neuron with linear activation function. The use of this activation function is justified by its effect on the learning process. Although nonlinear activation functions are proposed for recursive layers, they do not cope with the problem described by our data and often lead to undertraining or overtraining of the model. However, the ReLU function strongly generalizes the solution, which turns out to have a positive effect on the quality of the learning process. We illustrated the described process in the diagram in Fig. 1.

The input parameters included data interpolated to Jason's position from CODE, ESA, JPL, and UPC centers, longitude, UTC time in sine and cosine, latitude, solar zenith angle, as well as Kp and F10.7 indices. In order to provide optimal conditions for the learning process and the evaluation of our model, we decided that the learning set would be divided into three subsets: the training set, the testing set, and the validation set, with a ratio of 75:15:10.

The model was then compiled, entailing the definition of a loss function, an optimizer, and metrics for evaluating the model's performance during training. To reduce the impact of back propagation on our model, we used the adaptive gradient algorithm (AdaGrad) (Duchi et al. 6) optimizer with a loss function defined by mean squared error, and mean absolute error as a metric for assessing model quality. After the training process, the model was validated. To analyze performance of our model we generated global ionospheric maps in IONEX format with 2 h resolution, maintaining spatial resolution of standard GIM (Latitudes ±87.5° with 2.5° step; Longitudes ±180° with 5° step). Thereafter, the results were compared to the final IGS maps for the purpose of validation.

Validation

We divided the quality validation of our model into two stages: the first stage is to validate the machine learning process itself, and the second stage is to check the quality of positioning using our product. The evaluation of the learning process is mainly based on checking the correctness of the algorithm. As the basic parameter determining the quality of our model, we use the coefficient of determination R^2 (Mbarak et al. 26), which indicates the fit of the model to the learning data and takes the form:

$$R^2 = 1 - \frac{\sum_{i=1}^{n}(y_i - \hat{y}_i)^2}{\sum_{i=1}^{n}(y_i - \bar{y}_i)^2} \tag{2}$$

where y_i is the expected value from the data-set, $\hat{y}_i$ is the value obtained from the model's prediction, and $\bar{y}_i$ is the average value of y in the learning set.

The second parameter describing the quality of our model is the Root Mean Square Error (RMSE), which provides information about how far the values obtained from the model are relative to the reference values. It is defined as:

$$RMSE = \sqrt{\sum_{i=1}^{n} \frac{(\hat{y}_i - y_i)^2}{n}} \tag{3}$$

The second stage of validation was to use global ionospheric maps to perform positioning tests and then compare the results with those obtained using the IGS final products. To carry out this analysis, maps with 2-hour resolution were generated so that a direct comparison between the two products could be made. To perform the validation in the GNSS positioning domain, we used the RTKLIB (Takasu 40) software to determine the positions of IGS stations during a three selected quiet periods (January 23–29, 2016, March 16–23, 2022 and February 1–6, 2023) and on specific days during which geomagnetic storms occurred (March 17, 2015, November 4, 2021, April 23–24, 2023). Validation over days with a sudden changes in the distribution of electrons in the ionosphere is crucial. Modeling the state of the ionosphere during geomagnetic storms is a significant problem, especially due to the small amount of data describing such a state in the training set. We specifically chose these storms and quiet weeks to test how the model handles the fusion of maps that were part of the learning set and those that were outside the set. This allowed us to assess the interpolation and extrapolation ability of the model. In addition we used calm period from 2016 and storm period from 2015 in order to show ability of our model not only to fuse maps that are outside of training range (2005–2021), but also to show ability to merge and improve historical data. Positioning was conducted on code-based single-frequency measurements, utilizing CODE precise ephemerides (orbit and clock) and compared to the precise coordinates from weekly IGS solutions stored in Solution INdependent EXchange (SINEX) files. To ensure consistent positioning conditions using both the IGS product and our model (referred to as GUT model),

Fig. 2 The learning results of the trained model, showcasing a comparison between reference (Jason-derived TEC) and predicted values. The comparison results are depicted in blue, while the red color represents the straight line fitted to the resulting data

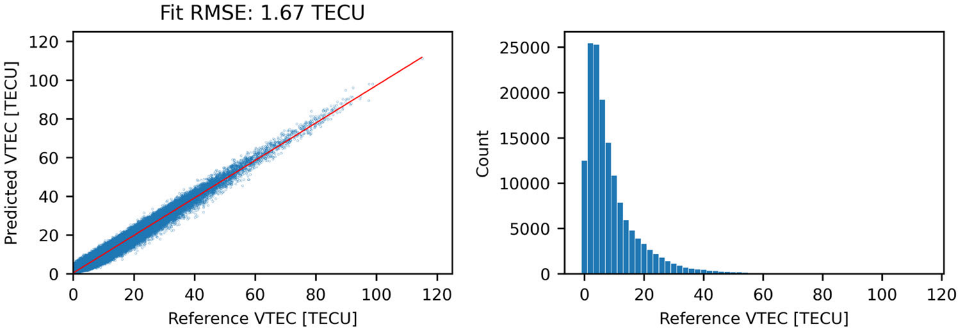

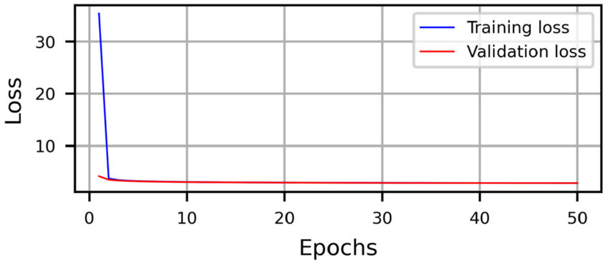

Fig. 3 A graph of the loss curve for the created model; the blue line shows the training curve and the red line shows the validation curve

we employed DCBs (as time group delay) from the navigation files for GPS and for GLONASS satellites. Using this parameters prepared in this manner, we determined the positions for over 300 IGS stations on selected storm days and during a calm periods.

Results

The results of learning model depend on three things in particular: the preparation of the dataset, the structure of the model and the selection of hyperparameters. As a first measure of the model quality, we used a comparison between the model's prediction results and the reference data. We obtained a low RMSE of 1.67 TECU and high R^2 score of 0.97, which indicates a high quality of the learning result. We presented a comparison between the reference data (Jason-derived TEC) in Fig. 2. These results show a disadvantage of the dataset, which is caused by the nature of the given input data. We noticed that our dataset contained mostly values ranging between 0–20 TECU, while number of points with higer values decreases proportionally with the increase of TEC. We did not found any significant deviations of predicted values from reference ones especially for higher TECs where we had smaller number of them in training dataset.

As a second metric of the quality of the learning process, we generated a loss curve. We noticed that as the number of epochs processed increased, the value decreased. Based on this, we decided to stop the learning process after 50 epochs due to the lack of performance improvement (Fig. 3). What is important at this stage is that we did not notice any signs of overtraining or undertraining of the model. This would be evident if, as the number of epochs processed increased, the loss of the validation set relative to the training set increased, or if the loss of the validation set was noticeably lower than the loss of the training set.

In Fig. 4, we show a comparison between the resulting predictions from the GUT model and the reference (Jason-derived TEC) and validation (IGS TEC) data from the test set. The average difference with respect to TEC from the altimetric measurements is -0.07 ± 1.67 TECU, while with respect to IGS it is 2.64 ± 0.99 TECU. These results show that the model satisfactorily fits the Jason's reference data. When examining the differences between Jason and GUT, we found a homogeneous distribution ranging mostly between -5.0 and 5.0 TECU, but when comparing IGS and GUT, we found that the differences are mostly positive, indicating lower TEC values from the GUT model. Based on the distribution of these differences, we noticed considerable variation in them for the solar maximum period (2012–2016).

To highlight the differences of ΔTEC for the IGS-GUT prediction, we performed the spatial comparison presented in Fig. 5. The vast majority of them are positive, indicating a general underestimation of values relative to the IGS. For the intertropical region they are smaller than for areas in the northern hemisphere, where we found an increase in differences. When comparing the altimetric measurements and the results from GUT model, we found that the negative values are mostly distributed in the northern and southern hemispheres above the parallels 23.5° North and South. In contrast, in the intertropical area, we recorded mostly positive difference values. This means that our model produces higher TEC for the equatorial areas while for the northern hemisphere and the southern polar circle it gives differences that are on average lower by 1.30 TECU. The differences obtained can be explained by the inaccuracy of TEC modeling above Jason's orbit. Despite the modeling of these values, this information does not perfectly reflect conditions for a given position at a given time. Presented results demonstrate that the data and learning method used are close to reference values and should reflect well the state of the ionosphere.

Discussion

During the learning process, we tried to adapt the model to fit the Jason-derived TEC as accurately as possible. As a result, the predictions obtained from it have a 98% correlation with the reference Jason measurement data. However, as is well known, the Jason measurements have certain limitations, such as the availability of data only for the seas and oceans and the lack of complete coverage of the polar regions. Therefore, the model must have excellent interpolation and extrapolation capabilities. To verify this, we decided to perform a comparison of single-frequency positioning results using IGS maps and the maps generated using the developed GUT model.

Quiet periods

For the purpose of validating the model during quiet periods, we selected weeks based on the average daily Kp and maximum daily solar disturbance. This information was obtained from the Aurora and Solar Activity Archive provided by GFZ German Research Centre for Geosciences (Matzka et al. 25). The validated periods are as follows: January 23–29, 2016; March 16–23, 2022; and February 1–6, 2023, where the maximum Kp index value does not exceed 4. It's worth noting that only the 2016 period was included in the model training data.

Figure 6 presents the cumulative distribution function for the RMSE for the three studied quiet periods. We noticed a considerable difference between the errors obtained for the altitude component of the topocentric coordinates. The results obtained with the GUT model for it (red line) show respective average improvements of 10.3% for January 23–29, 2016, 5.9% for the week of March 16–23, 2022, and 15.0% for February 1–6, 2023, relative to the IGS results. This translates directly to 3D positioning, where the average improvement in RMSE for the specified periods being 8.2%, 4.8%, and 12.0%, respectively. However, these results are negatively affected by the slight increase in errors for 2D positioning, which amounts to 1.6% for the period January 23–29, 2016, and slight average improvements of 0.6% and 2.1% for March 16–23, 2022 and February 1–6, 2023, respectively.

Fig. 4 Temporal comparison among test sets between prediction results and reference data (Jason-derived TEC) and validation data (IGS TEC)

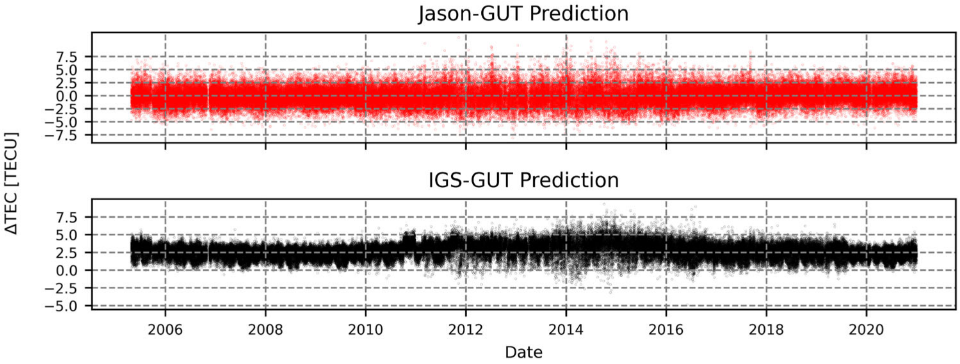

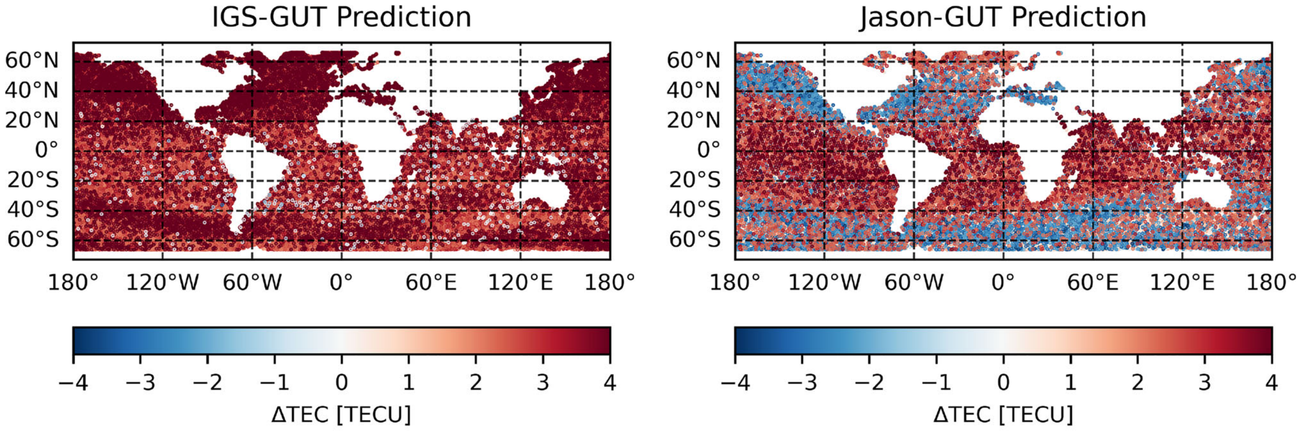

Fig. 5 Spatial comparison among test sets between prediction results and reference data (Jason-derived TEC) and validation data (IGS TEC)

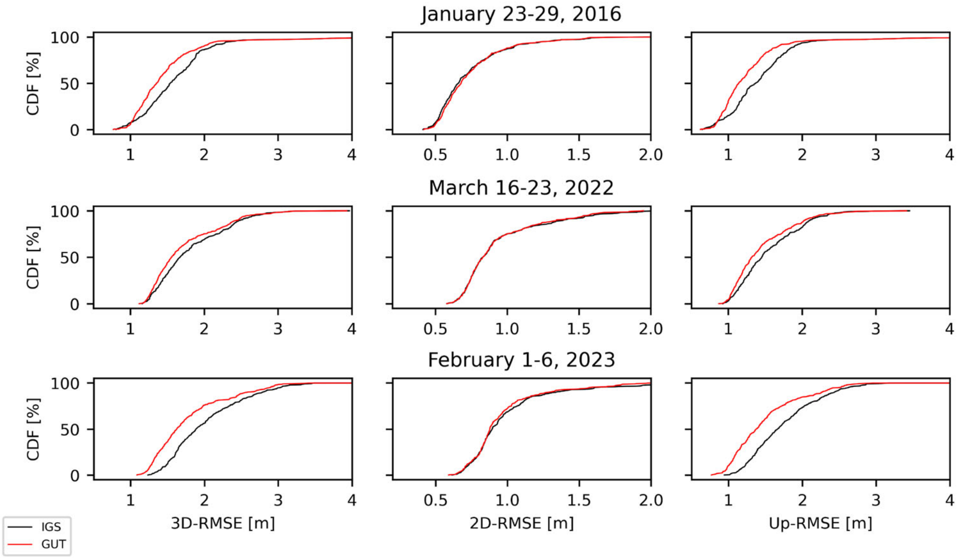

Fig. 6 Cumulative distribution functions graphs for the RMSE obtained from positioning for all available IGS stations for the studied quiet periods: January 23–29, 2016; March 16–23, 2022; February 1–6, 2023. The red line shows the results obtained using maps generated from the GUT model, while the black line shows the results obtained by using IGS maps

Figure 7 shows the distributions of improvement or deterioration of the 3D RMSE relative to the IGS results for selected quiet periods. We noticed that the results are not uniform, although some trends might be discerned. Significant improvements were recorded for stations located in the North and South America for all periods. We also found, that for each dates we got an improvement for stations close to polar regions. Out of the 332 stations for the 2023 period, 302 stations (91%) show improved 3D RMSE, while only 4 stations exhibit an error deterioration of more than 0.10 m. During the 2016 survey period, 301 stations were used in validation, with 74% of them showing improved positioning results, while for the 2022 period, it was 71%. It is worth noting that for the quiet periods in 2016 and 2023, more than 40 stations reached more than 20% 3D RMSE improvement.

The spatial range of the Jason satellite is limited to 66.15° N and 66.15° S. It means, that part of the analyzed stations are located outside this area and the result of their positioning may be burdened by incorrect modeling of the ionospheric state for these regions. For the quiet period in 2016, 21 stations reached an improvement of the 3D RMSE. For ten of them, the improvement was more greater equal than 20% (up to a maximum of 26%). Accuracy degradation was obtained for only one station and amounted to less than 1%. For other analyzed quiet periods the results were similar. For 2022, 23 stations with improvements up to 24% and only 5 with deterioration not greater than 6%. For 2023, all 19 stations achieved an improvement of 6–39%. In general, we were able to obtain average percentage improvements for the studied calm dates of 11% for the northern polar region and 22% for the southern polar region. This proves that the developed model performs well in extrapolating data beyond Jason's coverage areas. In the Appendix A we provided the information regarding 3D RMSE deterioration and improvement for calm periods for GNSS stations that are outside of Jason's area of operation.

More detailed information about the distribution of the improvements or deteriorations compared to the IGS solution are presented in Fig. 8. The figure shows the difference between the positioning RMSE obtained using IGS and GUT maps. A positive value of the difference indicates an improvement, while a negative value indicates a deterioration for the studied stations. For each of the quiet terms tested, we obtained an improvement in 3D positioning. In the figure, the range of improvements obtained in the form of percentiles, where we will refer the 25th percentile as Q1 and the 75th as Q3. The median was 0.14 m with Q1 of 0.00 m and Q3 of 0.29 m for January 23–29, 2016, 0.07 m with Q1 of −0.01 m and Q3 of 0.17 m for March 16–23, 2022, and 0.22 m with Q1 of 0.10 m and Q3 of 0.34 m for February 1–6, 2023. The medians of the positioning errors according to the altitude component are close to the 3D results. The medians, Q1 and Q3 for each of the studied periods are higher than zero. For 2D positioning the medians are close to zero, indicating a high degree of similarity to IGS. The obtained results indicate that the use of the GUT model for the generation of ionospheric maps enables a general improvement of the single-frequency positioning for the quiet state of the ionosphere.

Positioning results for individual stations depend on their location and ionospheric conditions. In order to check the quality of positioning for individual stations on a different latitudes with various densities of surrounding stations, we present the time series of positioning errors in the North, East and Up directions for the SCOR (Greenland; 70.5° N 22.0° W), STR1 (Australia; 35.3° S 149.0° E) and LROC (France; 46.2° N 1.2° E) stations as shown in Fig. 9. The error values obtained with the GUT model in each direction are very similar to the IGS results. However, a certain improvement is

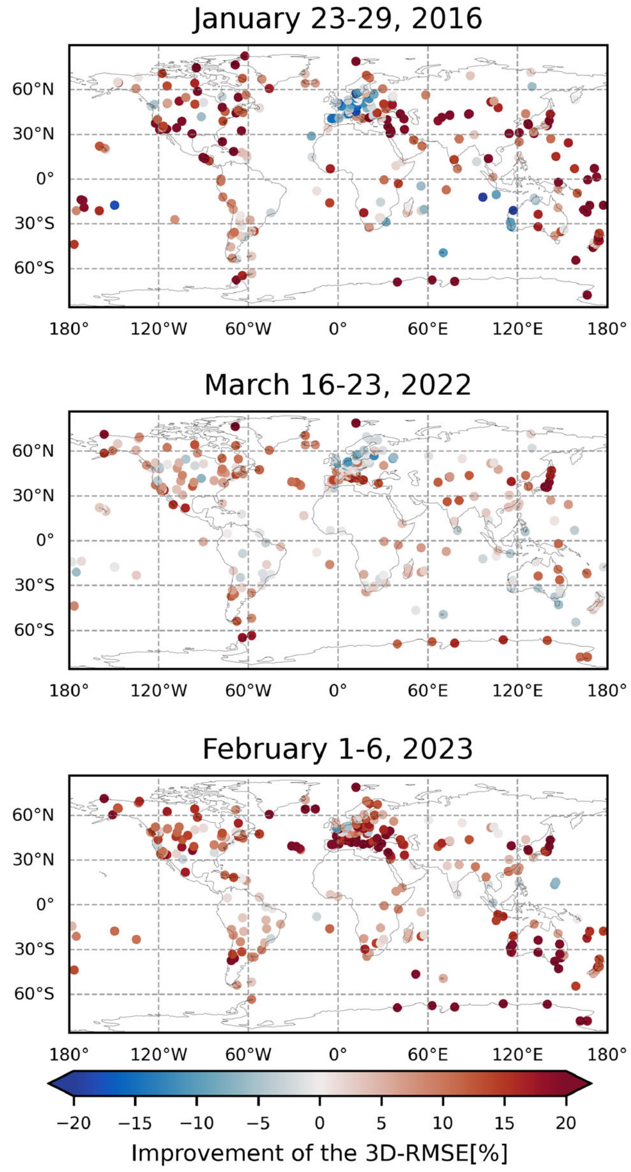

Fig. 7 Spatial distribution of stations showing improvement or deterioration with respect to IGS for the studied quiet periods: January 23–29, 2016, March 16–23, 2022 and February 1–6, 2023

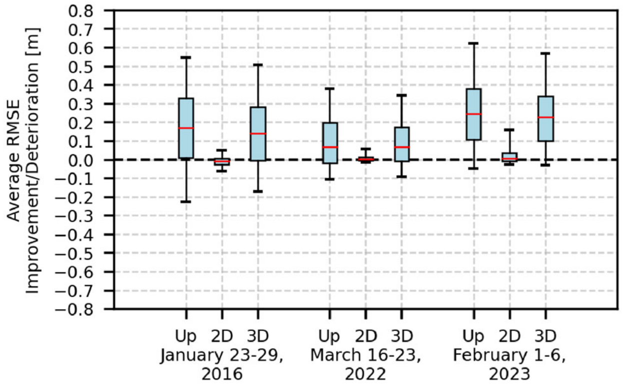

Fig. 8 Comparison of the improvements and deterioration of the GUT model against the IGS solution for Up, 2D, 3D positioning error for the studied quiet periods: January 23–29, 2016, March 16–23, 2022, February 1–6, 2023. The red line represents the median, the bottom and top of the box indicate the 25th and 75th percentile while the whiskers, lower and upper, indicate the 5th and 95th percentile respectively

noticeable. This is particularly evident during the first three days of the observation period for station STR1, where a significant improvement in positioning in the North and Up directions is visible. For the entire week, the average altitude error for the GUT model was 0.22 ± 1.58 m, while for the IGS model it was -0.81 ± 1.85 m. In the north and east directions, the improvements are not as pronounced, although we noticed centimeter improvements in standard deviation (std), of 0.04 m and 0.03 m respectively. For the SCOR station, there is a slight bias against the IGS results. It is particularly pronounced for the altitude component, where GUT shows an average of 0.37 ± 1.54 m, and IGS -0.61 ± 1.55 m. For the LROC station, we obtained a bias between the GUT and IGS results of 0.80 m for altitude. For the GUT model the standard deviation decreased slightly, by 0.03 m. However, considering the RMSE, we noted a significant improvement, 0.87 m for the GUT model and 1.26 m for the IGS.

Storm events

In order to validate the model for periods with increased ionospheric activity, we selected such days during which geomagnetic storms were recorded. The validated periods are as follows: March 17, 2015 (Wu et al. 42), November 4, 2021 (Zhai et al. 45; Wu et al. 43), April 23–24, 2023. During each of these storms, the Kp index value reached 8 in a scale of 0 to 10. We chose such extreme storm dates to test the quality of the model under the worst conditions. It should be noted that the events in November 2021 and April 2023 were outside the range of data used to train the model.

In Fig. 10 we noticed a similar pattern as in the analysis of the calm days. For each of the selected storms, we obtained a better average improvements for 3D positioning while compared to IGS (March 17, 2015: 12.9%; November 4, 2021: 8.5%; April 23–24, 2023: 11.5%). For 2D positioning errors we obtained similar results to IGS. This is another evidence that the applied method performs effectively in mapping changes in the state of the ionosphere. The results show that on days with strong geomagnetic disturbances, we get comparable 2D positioning results using the GUT model as with final IGS products, and we get better results for the altitude component.

Figure 11 shows the distribution of improvements and deterioration in the positioning RMSE for the available IGS stations during selected periods when strong geomagnetic disturbances were recorded. In the case of ionospheric storms, their magnitude and area of occurrence should be taken into account. We obtained very good positioning results for the strongest storm of the 24th solar cycle (March 17, 2015). Out of 269 stations analyzed on a given day, we found an improvement for 209 of them (78%), while only 27 (10%) stations experienced a degradation of more than 0.10 m during the storm. The April 2023 storm shows similar statistics, where out of 334 stations we noticed an improvement for 288 of them (86%). A slightly lower number of improved results was obtained for the November 2021 storm, where out of 323 stations considered in the calculations, 224 received lower positioning errors than when using the IGS maps (69%). An important issue in the development of the fusion model is the consideration of the extreme behavior of the ionosphere. Of the 16 years of data used in the study, only a few describe the ionosphere in an excited state, which could be reflected in model accuracy during intense geomagnetic activity. Nevertheless, the maps generated by the GUT model allow to improve on average 70% of the stations for the studied storm days.

When analyzing the percentage improvement in 3D positioning results for days of geomagnetic disturbances, we noticed that for storms from 2015 and 2023, more than 70 stations achieved more than 15% improvement.

Likewise for the calm days, also for the storm events we noticed good performance of the model for the GNSS stations located on northern and southern polar regions (Fig. 11). For the March 2015 storm, 22 stations achieved 3D RMSE improvements ranging from 3 to 26% (average 18%), and only 3 stations showed minor degradation not exceeding 5%. For the 2021 storm, 24 stations with an average improvement of about 13%, and only 5 stations with average deterioration around 1.4%. For the event in 2023, all 19 stations reached significant 3D positioning improvement about 17% on average. For the northern polar region, the average percentage improvement for all of the storms was 13%, while for the southern polar region it was 15%. This shows that the developed model does a very good job of extrapolating data beyond the Jason range for both calm and stormy periods. We have presented more detailed information regarding the quality of positioning using the GUT model for stations outside the Jason satellite operating area on storm days in the Appendix A.

Figure 12 represents the RMSE statistics of positioning using the GUT in relation to the IGS model for days with strong geomagnetic activity. We noticed a similar results as in for quiet period (Fig. 8). For the March 17, 2015, the 3D median was 0.20 m (Q1 of 0.02 m; Q3 of 0.39 m), for November 4, 2021, the median was 0.07 m (Q1 of −0.02 m; Q3 of 0.15 m) and for April 23–24, 2023 it was 0.20 m (Q1 of 0.08 m; Q3 of 0.23 m). The 3D medians obtained for each date were positive, and the Q1 values are close to zero, implying that improvements were achieved for the vast majority of stations studied. We obtained similar results for the altitude component. This median was 0.25 m, 0.08 m and 0.25 m for March 17, 2015, November 4, 2021 and April 23–24, 2023, respectively. The 2D positioning medians are close to zero with slight centimeter deviations.

In order to validate how the model performs with TEC mapping during a storm day, we decided to choose one station that was in the center of the impact of ionospheric disturbances (Zhai et al. 45), which is the SPTU located in southern Brazil. In Fig. 13 we showed the daily course of the components of the topocentric coordinates. Our results do not deviate much from the IGS results, especially for the quiet part of the day. It should also be taken into account that we are in the middle of the land, where the model had to interpolate the data. According to the information in (Zhai et al. 45), the disturbance started at 11:00 UTC and lasted until 18:00 UTC. The results we obtained differ slightly from the IGS for this period for each of the components. The average positioning error in the East direction for the GUT model is 0.22 m and for IGS is 0.25 m, where the std is almost the same ±0.86 and ±0.90 m respectively. In the North direction the GUT model is characterized by a 4 cm deterioration in the average error relative to IGS and a 5 cm improvement in the standard deviation. For altitude it turns out that the IGS solution performs better, as for the mean error using GUT is 0.85 m, while with IGS it is 0.35 m, which is quite a difference. However, we gained 0.18 m improvement in the standard deviation, which for our model is ±2.12 m.

Impact of plasmaspheric TEC correction

During investigation we noticed that the plasmaspheric model selection has a strong impact on the learning results. The Jason satellites orbit at an altitude of 1336 km. In contrast, the ionospheric maps from the IAACs use GNSS measurements where the satellites are in orbits at altitudes above 20000 km. This means that the altimetric measurements ignore the influence of the ionosphere above Jason's orbit resulting an underestimation of plasmaspheric total electron content. Therefore, it was important to complement the data with TEC above Jason's orbit. In the course of our research, we examined models such as IRI2016 (Bilitza et al. 2), IRIPLAS (Sezen et al. 39), NEDM (Hoque et al. 18) and solution without ionospheric correction. We obtained the best results using the NEDM model. In Fig. 14, we showed the positioning statistics using different sources of plasmaspheric correction. If no correction is applied we found a significant deterioration of the positioning compared to the IGS, reaching even more than 15% for 3D positioning during a geomagnetic storm. The use of an appropriate model was crucial. The IRI2016 model brought an improvement in the results, but it was not satisfactory due to the numerous deterioration's that occurred. We found that on average model performed better for 55% of the stations, where the

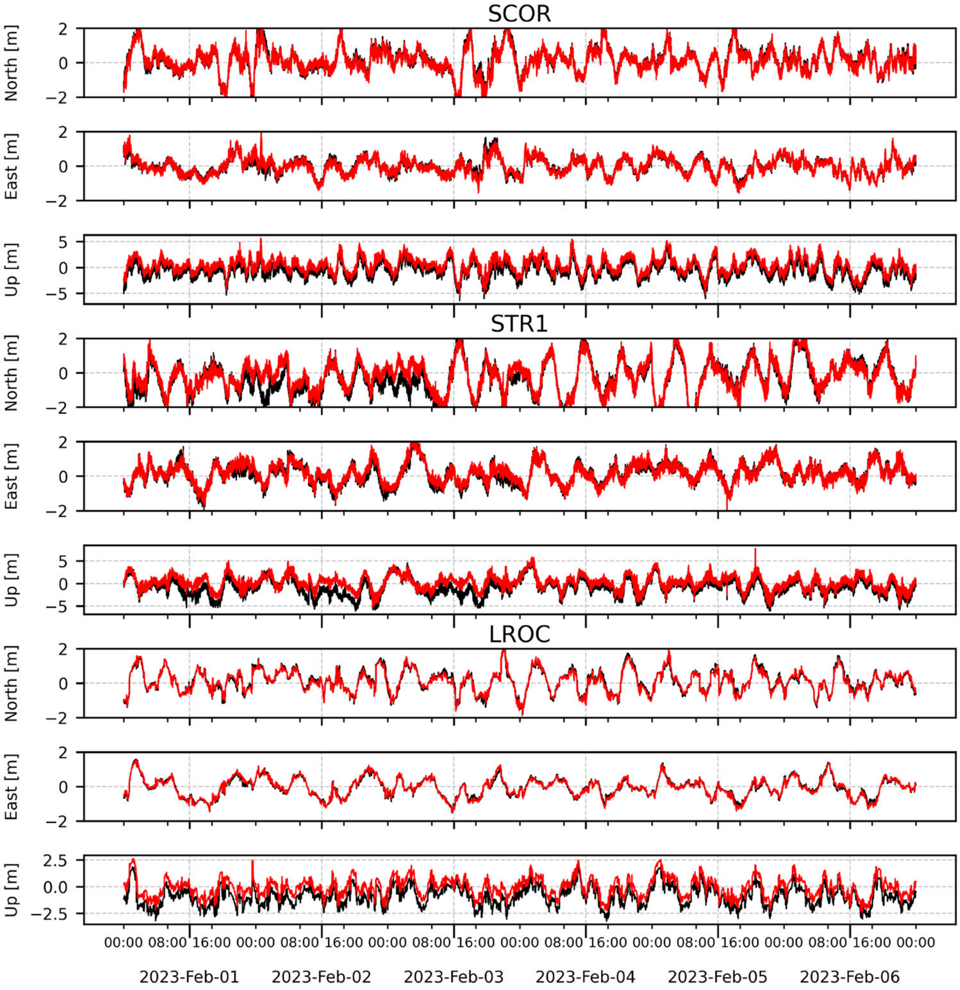

Fig. 9 Time series of topocentric coordinates for the period February 1–6, 2023, showing positioning results using the GUT product (red line) and IGS (black line); SCOR station; STR1 station; LROC station

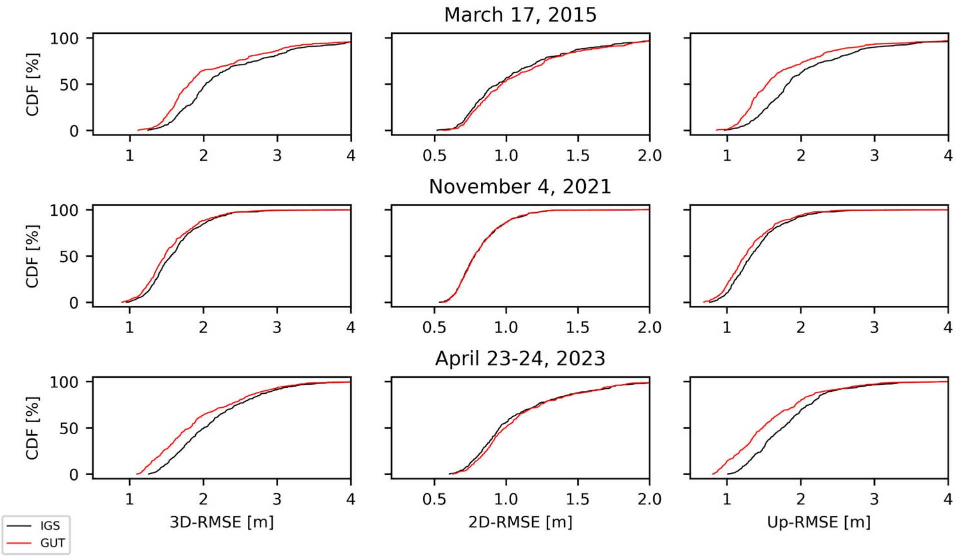

Fig. 10 Cumulative distribution function for the RMSE distribution of positioning for all available IGS stations during the studied storm periods: March 17, 2015, November 4, 2021 and April 23–24, 2023. The red line represents results obtained using maps generated from the GUT model, while the black line represents results obtained using IGS maps

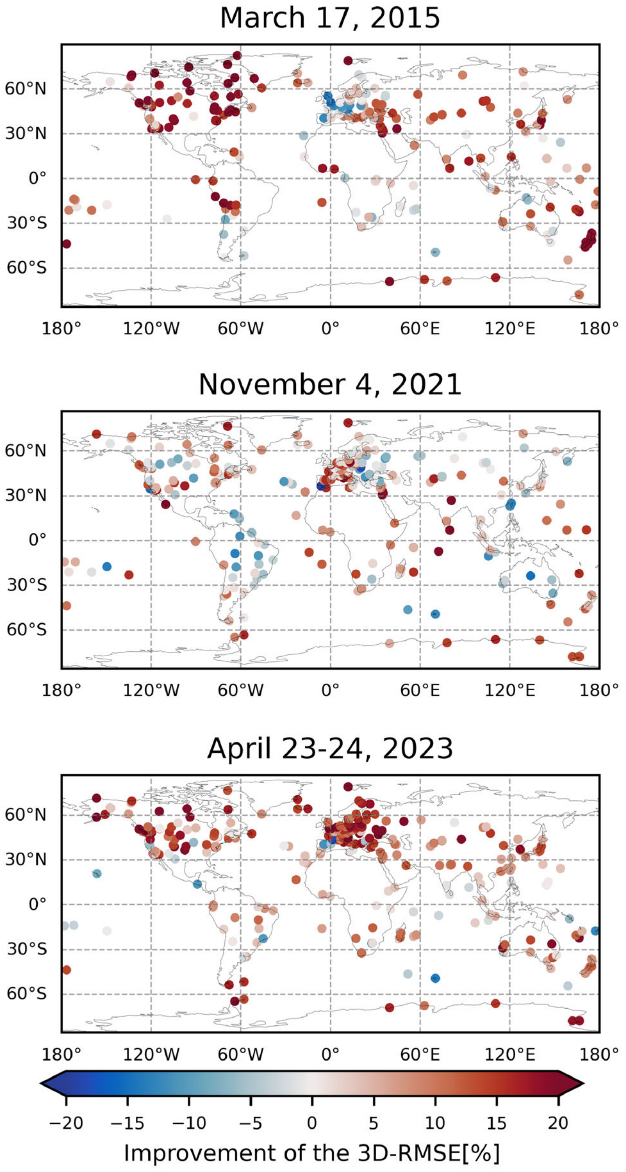

Fig. 11 Spatial distribution of stations showing improvement or deterioration with respect to IGS for the studied geomagnetic storm days: March 17, 2015; November 4, 2021; April 23–24, 2023

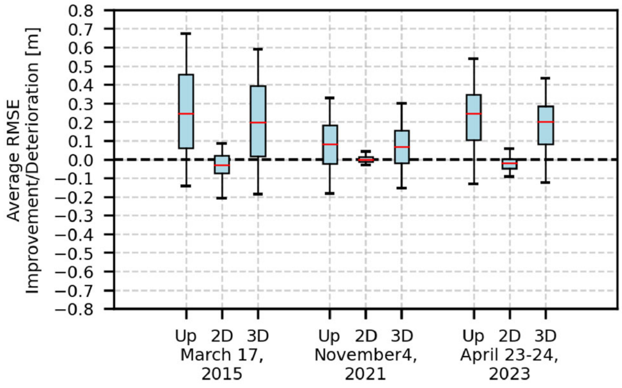

Fig. 12 Comparison of the improvements and deterioration of the GUT model against the IGS solution for Up, 2D, and 3D positioning error for the studied storm periods: March 17, 2015, November 4, 2021, and April 23–24, 2023. The red line represents the median, the bottom and top of the box indicate the 25th and 75th percentile while the whiskers, lower and upper, indicate the 5th and 95th percentile respectively

worst results were obtained for November 4, 2021 storm. For this day we only got better results for 33% of the station with an average 9.4% deterioration of 3D RMSE. We noticed that the corrections were underestimated when using IRI2016. The use of IRIPLAS proved to be more successful, where we obtained significant improvements by increasing the plasmapheric corrections. On average 65% exhibited reduction in 3D RMSE. Unfortunately, the use of this model still yielded some degradation, especially for 2D positioning, which reached up to 6.4% of deterioration in relation to IGS results. The use of the NEDM model proved to be a success and it performed best for all the dates analyzed, both calm and storm days. The results obtained minimizing errors in 2D positioning, which allows us to obtain results comparable to and better than IGS at this point. We found improvement for more than 70% of the studied station with average 7.9% reduction of 3D RMSE in relation to results obtained using final IGS products.

Fig. 13 Time series of topocentric coordinates of the SPTU station located in the area of influence of the storm on November 4, 2021. The red line shows the results obtained using maps generated with the GUT model, while the black line represents the IGS results

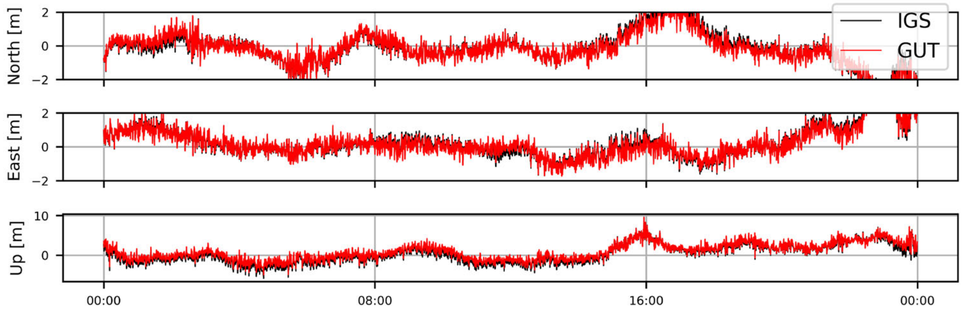

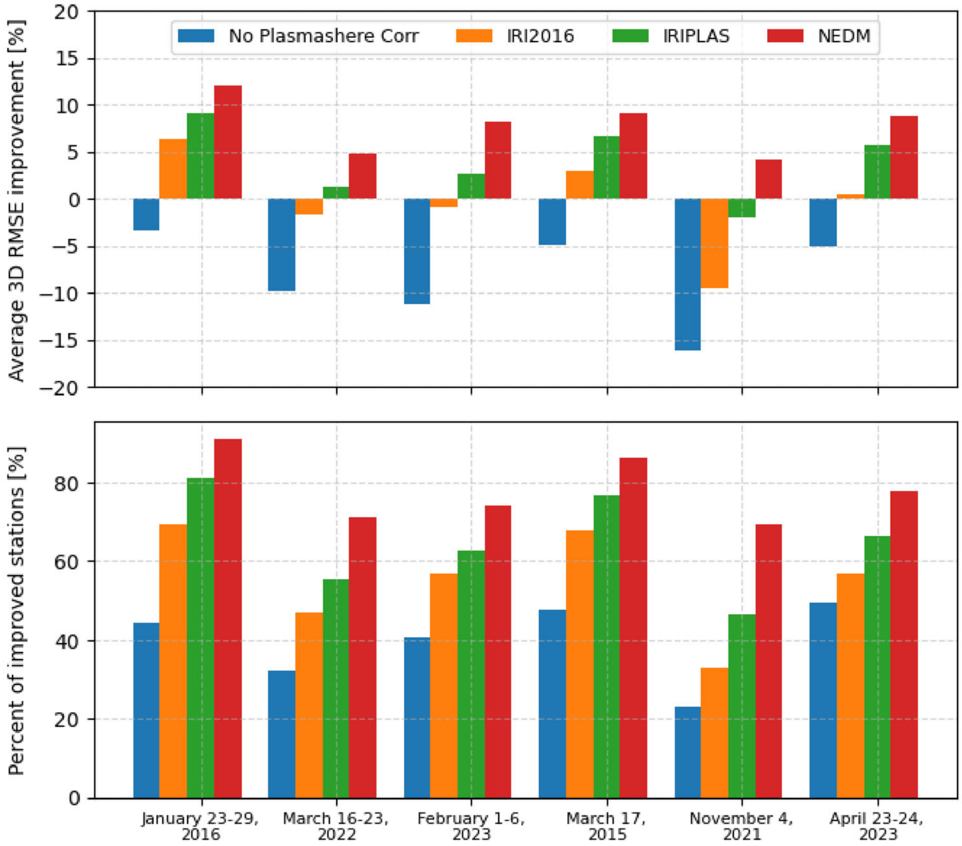

Fig. 14 Comparison of average 3D RMSE improvements for different applied plasmaspheric TEC corrections with respect to solution using final IGS GIM. Blue: no plasmaspheric correction, orange: IRI2016 model, green: IRIPLAS model, red: NEDM

Summary

The objective of our work was to develop a deep learning model that could be used to combine global ionospheric maps from different IAACs, and provide a high-quality end product. To construct the GUT model, we used a deep learning structure consisting of recursive layers and standard dense layers. Algorithm was fed with learning data, which consisted of TEC values from IAACs (CODE, ESA, JPL, UPC) interpolated to the Jason position, parameters representing UTC time, positional parameters representing solar zenith angle, latitude and longitude, and solar and geomagnetic activity parameters. Our model was validated in the positioning domain for different quiet and active solar periods using IGS GNSS stations located worldwide. Subsequently, the results were compared to those obtained using the final IGS products.

The proposed deep learning-based model achieved a significant reduction in GNSS positioning errors compared to the reference model, demonstrating its effectiveness in capturing complex spatio-temporal patterns within the input GIMs. Although the approach differs from the IGS solution in both methodology and input data, the results highlight the potential of deep learning-based technique to enhance existing ionospheric modeling strategies. Utilization of developed model for the selected quiet and storm days resulted in an improvement of the 3D positioning error (in comparison to the application of the final IGS solution) for over 70% of the investigated stations. This is mainly due to a notable enhancement in the accuracy of the altitude component, while the results for 2D positioning are comparable to those of the IGS.

Our results proves that the that the application of deep learning enables the combination of ionospheric maps from different IAACs, providing an ionospheric state that allows for improved positioning accuracy. Despite the model being trained using data from Jason satellites as a reference VTEC values, which are only available for the oceans, the positioning results demonstrate that even stations located deep within terrestrial areas exhibit enhanced positioning accuracy. A similar situation arises for the stations situated in the polar regions, where the altimetry data are unavailable. This demonstrates that the model is highly effective at extrapolating data beyond the range of the reference data. In our research, we also tested the impact of plasmaspheric models that were necessary to complete Jason's data above the satellite's orbit. The results show that the NEDM model allowed to improve learning process and improved positioning for twice as many stations as in the absence of the spherical plasma correction. Further advancement can be achieved by fusing data from different sources. The developed model can not only successfully improve the combination of current ionospheric maps, but also be applied to improve historical solutions.

Appendix A Percentage improvement/deterioration in 3D RMSE using the GUT model against the IGS model for GNSS stations located outside Jason domain

Station	Lat.[°]	Lon.[°]	Jan. 23–29 2016	Mar. 16–23 2022	Feb. 1–6 2023	Mar. 17 2015	Nov. 4 2021	Apr. 23–24 2023
ALRT	82.5	− 62.3	19.1	–	–	20.6	–	–
NABG	78.9	11.9	–	20.0	–	–	16.4	–
NYA2	78.9	11.9	–	23.6	24.5	–	19.8	32.1
NYA1	78.9	11.9	19.9	19.9	20.7	23.4	17.3	29.0
THU3	76.5	− 68.8	22.5	–	–	25.3	–	–
THU2	76.5	− 68.8	25.4	19.9	–	25.7	16.8	12.8
RESO	74.7	− 94.9	21.0	–	–	26.5	–	–
TIXI	71.6	128.9	2.1	–	–	7.2	3.8	–
TIXG	71.6	128.9	1.7	2.2	–	3.7	6.6	–
UTQI	71.3	− 156.6	–	19.5	26.3	–	15.4	23.0
HOLM	70.7	− 117.8	13.9	–	–	22.6	–	–
SCOR	70.5	− 22.0	3.5	10.2	5.8	5.8	7.1	16.4
TRO1	69.7	18.9	12.5	–1.7	10.1	–2.4	3.9	15.3
NRIL	69.4	88.4	3.3	–	–	9.0	− 0.1	–
TUKT	69.4	− 133.0	–	8.4	16.2	23.9	9.7	15.7
INVK	68.3	− 133.5	0.6	3.2	10.8	18.0	4.0	5.0
KIR0	67.9	21.1	9.6	− 2.4	14.5	− 1.1	− 0.3	17.0
KIR8	67.9	21.1	–	− 4.1	12.9	–	− 0.3	16.1
KIRU	67.9	21.0	− 0.9	− 6.0	8.8	− 5.1	− 6.2	10.3
QIKI	67.6	− 64.0	12.0	–	–	24.7	–	–
SOD3	67.4	26.4	–	− 2.2	12.6	–	− 0.1	18.4
KELY	67.0	− 50.9	7.6	–	–	19.5	–	–
CAS1	− 66.3	110.5	–	16.2	34.0	16.7	16.4	15.2
DUMG	− 66.7	140.0	–	13.4	32.0	–	12.9	–
ROTH	− 67.6	− 68.1	19.4	–	–	–	–	–
MAW1	− 67.6	62.9	25.0	12.2	36.2	15.6	–	10.6
DAV1	− 68.6	78.0	22.5	16.0	38.1	12.5	14.5	–
SYOG	− 69.0	39.6	26.1	11.4	39.2	19.4	5.5	16.5
COTE	− 77.8	162.0	–	10.8	23.1	–	13.4	17.8
ARHT	− 77.8	166.7	–	11.6	19.1	–	13.6	18.2
SCTB	− 77.8	166.8	–	13.8	–	–	17.4	20.8
MCM4	− 77.8	166.7	20.2	9.8	16.1	10.5	12.0	17.1

Acknowledgements Calculations were carried out at the Academic Computer Centre in Gdańsk.

Author Contributions Conceptualization, MP and GN; methodology, MP, GN and MMH; software, MP; validation, GN and MMH; formal analysis, MP, GN and MMH; investigation, MP and GN; resources, MP; data curation, MP; writing-original draft preparation, MP; writing-review and editing, GN, MMH and JS; visualization, MP and GN; supervision, GN, MMH and JS; project administration, GN; funding acquisition, GN. All authors have read and agreed to the published version of the manuscript.

Funding MP and GN acknowledge support from the Gdańsk University of Technology by the DEC-31/2021/IDUB/I.3.3 grant under the ARGENTUM-"Excellence Initiative-Research University" program.

Availability of data and materials Total electron content data derived from the Jason satellites were downloaded from Open Altimeter Database (OpenADB) (https://openadb.dgfi.tum.de/en/, accessed on 22 October 2021). GNSS global ionospheric maps were collected from Crustal Dynamic Data Information System (CDDIS) (https://cddis.nasa.gov/, accessed on 15 October 2021). The datasets containing TEC differences between Jason-derived TEC and GIMs are available from the corresponding author on reasonable request. The data is not publicly available due to privacy reasons.

Declarations

Conflict of interest The authors declare no conflict of interest.

Code availability The code for deep learning model is available from the corresponding author on reasonable request. The code is not publicly available due to privacy reasons.

References

Badulin SI, Grigorieva VG, Shabanov PA et al (2021) Sea state bias in altimetry measurements within the theory of similarity for wind-driven seas. Adv Space Res 68(2):978–988. https://doi.org/10.1016/j.asr.2019.11.040

Bilitza D, Altadill D, Truhlik V et al (2017) International reference ionosphere 2016: from ionospheric climate to real-time weather predictions. Space Weather 15(2):418–429. https://doi.org/10.1002/2016SW001593

Chen Z, Zhou K, Li H et al (2023) Global TEC map fusion through a hybrid deep learning model: RFGAN. Space Weather 21(1):e2022SW003341. https://doi.org/10.1029/2022SW003341

Chollet F et al (2015) Keras. https://keras.io

Dettmering D, Schmidt M, Heinkelmann R et al (2011) Combination of different space-geodetic observations for regional ionosphere modeling. J Geod 85(12):989–998. https://doi.org/10.1007/s00190-010-0423-1

Duchi J, Hazan E, Singer Y (2011) Adaptive subgradient methods for online learning and stochastic optimization. J Mach Learn Res 12:2121–2159

European Commission (2016) European GNSS (Galileo) open service—ionospheric correction algorithm for Galileo single frequency users, issue 1.2. Technical report, European Commission. https://www.gsc-europa.eu/electronic-library/programme-reference-documents

European Union (2022) NTCM-G ionospheric model description, issue 1.0. Technical report, European Union. https://www.gsc-europa.eu/support-to-developers/ionospheric-correction-algorithms/galileo-ntcm-g-source-code

Feltens J (1998) Chapman profile approach for 3-d global TEC representation. IGS presentation, pp 285–297

Feltens J (2007) Development of a new three-dimensional mathematical ionosphere model at European Space Agency/European Space Operations Centre. Space Weather. https://doi.org/10.1029/2006SW000294

Galkin IA, Reinisch BW, Huang X et al (2012) Assimilation of GIRO data into a real-time IRI. Radio Sci. https://doi.org/10.1029/2011RS004952

Gardner LC, Schunk RW, Scherliess L et al (2014) Global assimilation of ionospheric measurements-Gauss Markov model: improved specifications with multiple data types. Space Weather 12(12):675–688. https://doi.org/10.1002/2014SW001104

Geron A (2019) Hands-on machine learning with Scikit-learn, Keras, and TensorFlow, 2nd edn. O'Reilly Media, Sebastopol, CA

Ghoddousi-Fard R, Héroux P, Danskin D et al (2011) Developing a GPS TEC mapping service over Canada. Space Weather. https://doi.org/10.1029/2010SW000621

Gonzalez WD, Tsurutani BT, Clúa de Gonzalez AL (1999) Interplanetary origin of geomagnetic storms. Space Sci Rev 88(3):529–562. https://doi.org/10.1023/A:1005160129098

Hernández-Pajares M, Juan J, Sanz J (1999) New approaches in global ionospheric determination using ground GPS data. J Atmos Solar Terr Phys 61(16):1237–1247. https://doi.org/10.1016/S1364-6826(99)00054-1

Hernández-Pajares M, Juan JM, Sanz J et al (2009) The IGS VTEC maps: a reliable source of ionospheric information since 1998. J Geod 83(3):263–275. https://doi.org/10.1007/s00190-008-0266-1

Hoque MM, Jakowski N, Prol FS (2022) A new climatological electron density model for supporting space weather services. J Space Weather Space Clim 12:1. https://doi.org/10.1051/swsc/2021044

Huang Z, Yuan H (2014) Research on regional ionospheric TEC modeling using RBF neural network. Sci China Technol Sci 57(6):1198–1205. https://doi.org/10.1007/s11431-014-5550-0

Klobuchar JA (1987) Ionospheric time-delay algorithm for single-frequency GPS users. IEEE Trans Aerosp Electron Syst AES 23(3):325–331. https://doi.org/10.1109/TAES.1987.310829

Li Z, Yuan Y, Wang N et al (2015) SHPTS: towards a new method for generating precise global ionospheric TEC map based on spherical harmonic and generalized trigonometric series functions. J Geod 89(4):331–345. https://doi.org/10.1007/s00190-014-0778-9

Liu Z, Li Y, Guo J et al (2016) Influence of higher-order ionospheric delay correction on GPS precise orbit determination and precise positioning. Geod Geodyn 7(5):369–376. https://doi.org/10.1016/j.geog.2016.06.005

Luo X, Gu S, Lou Y et al (2018) Assessing the performance of GPS precise point positioning under different geomagnetic storm conditions during solar cycle 24. Sensors. https://doi.org/10.3390/s18061784

Mannucci AJ, Wilson BD, Yuan DN et al (1998) A global mapping technique for GPS-derived ionospheric total electron content measurements. Radio Sci 33(3):565–582. https://doi.org/10.1029/97RS02707

Matzka J, Stolle C, Yamazaki Y et al (2021) The geomagnetic kp index and derived indices of geomagnetic activity. Space Weather 19(5):e2020SW002641. https://doi.org/10.1029/2020SW002641

Mbarak WK, Cinicioglu EN, Cinicioglu O (2020) SPT based determination of undrained shear strength: regression models and machine learning. Front Struct Civ Eng 14(1):185–198. https://doi.org/10.1007/s11709-019-0591-x

Nava B, Coïsson P, Radicella S (2008) A new version of the Nequick ionosphere electron density model. J Atmos Sol-Terr Phys 70(15):1856–1862. https://doi.org/10.1016/j.jastp.2008.01.015. (**Ionospheric effects and telecommunications**)

Nencioli F (2021) SALP-RP-MA-EA-23407-CLS: filtering ionospheric correction from altimetry dual-frequencies solution. Technical rep, CLS

Pedregosa F, Varoquaux G, Gramfort A et al (2011) Scikit-learn: machine learning in Python. J Mach Learn Res 12:2825–2830

Peng T, Wang D, Jia X, et al (2019) Impact of the ionosphere and GPS surveying caused by coronal mass ejection on May 23 (2017). In: Sun J, Yang C, Yang Y (eds) China Satellite Navigation Conference (CSNC) 2019 proceedings. Springer, Singapore, pp 325–336

Poniatowski M, Nykiel G (2020) Degradation of kinematic PPP of GNSS stations in central Europe caused by medium-scale traveling ionospheric disturbances during the St. Patrick's day 2015 geomagnetic storm. Remote Sens. https://doi.org/10.3390/rs12213582

Poniatowski M, Nykiel G, Borries C et al (2023) Spatio-temporal validation of GNSS-derived global ionosphere maps using 16 years of Jason satellites observations. Remote Sens 15:20. https://doi.org/10.3390/rs15205053

Qian L, Burns AG, Emery BA, et al (2014) The NCAR TIE-GCM, American Geophysical Union (AGU), chap 7, pp 73–83. https://doi.org/10.1002/9781118704417.ch7

Razin M, Voosoghi B, Mohammadzadeh A (2016) Efficiency of artificial neural networks in map of total electron content over Iran. Acta Geod Geophys 51(3):541–555. https://doi.org/10.1007/s40328-015-0143-3

Richards PG (2001) Seasonal and solar cycle variations of the ionospheric peak electron density: comparison of measurement and models. J Geophys Res Space Phys 106(A7):12803–12819. https://doi.org/10.1029/2000JA000365

Schaer S, Beutler G, Rothacher M, et al (1996) Daily global ionosphere maps based on GPS carrier phase data routinely produced by the code analysis center. In: Proceedings of the IGS analysis center workshop 1996

Schaer S, Gurtner W, Feltens J (1998) Ionex: the ionosphere map exchange format version 1. In: Proceedings of the IGS AC workshop, Darmstadt, Germany, pp 233–247

Scharroo R, Smith WHF (2010) A global positioning system-based climatology for the total electron content in the ionosphere. J Geophys Res Space Phys. https://doi.org/10.1029/2009JA014719

Sezen U, Gulyaeva T, Arikan F (2018) Online computation of international reference ionosphere extended to plasmasphere (IRI-Plas) model for space weather. Geod Geodyn 9(5):347–357. https://doi.org/10.1016/j.geog.2018.06.004

Takasu T (2007–2013) RTKLIB: an open source program package for RTK-GPS. http://gpspp.sakura.ne.jp/rtklib/rtklib.htm

Wen Z, Li S, Li L et al (2021) Ionospheric TEC prediction using long short-term memory deep learning network. Astrophys Space Sci 366(1):3. https://doi.org/10.1007/s10509-020-03907-1

Wu CC, Liou K, Lepping RP et al (2016) The first super geomagnetic storm of solar cycle 24: “the St. Patrick’s day event (17 March 2015)”. Earth Planets Space 68(1):151. https://doi.org/10.1186/s40623-016-0525-y

Wu Q, Wang W, Lin D et al (2024) Penetrating electric field during the Nov 3–4, 2021 geomagnetic storm. J Atmos Solar Terr Phys 257:106219. https://doi.org/10.1016/j.jastp.2024.106219

Yasukevich YV, Afraimovich EL, Palamarchuk KS et al (2009) Testing of the international reference ionosphere model using the data of dual-frequency satellite altimeters “Topex”/“Poseidon” and “Jason-1”. Radiophys Quantum Electron 52(5):341. https://doi.org/10.1007/s11141-009-9137-8

Zhai C, Tang S, Peng W et al (2023) Driver of the positive ionospheric storm over the South American sector during 4 November 2021 geomagnetic storm. Remote Sens. https://doi.org/10.3390/rs15010111

Zhang H, Xu P, Han W et al (2013) Eliminating negative VTEC in global ionosphere maps using inequality-constrained least squares. Adv Space Res 51(6):988–1000. https://doi.org/10.1016/j.asr.2012.06.026

Zhukov AV, Yasyukevich YV, Bykov AE (2020) GIMLi: global ionospheric total electron content model based on machine learning. GPS Solut 25(1):19. https://doi.org/10.1007/s10291-020-01055-1